Nanotechnology **19** (2008) 395302 (5pp) doi:10.1088/0957-4484/19/39/395302

Full-field hard x-ray microscopy below 30 nm: a challenging nanofabrication achievement

Yu-Tung Chen[1,2], Tsung-Nan Lo[1], Yong S Chu[3], Jaemock Yi[3], Chi-Jen Liu[1], Jun-Yue Wang[1], Cheng-Liang Wang[1], Chen-Wei Chiu[1], Tzu-En Hua[1], Yeukuang Hwu[1,4,5,6], Qun Shen[3], Gung-Chian Yin[6], Keng S Liang[6], Hong-Ming Lin[2], Jung Ho Je[7] and Giorgio Margaritondo[8,9]

[1] Institute of Physics, Academia Sinica, Taipei 115, Taiwan
[2] Department of Materials Engineering, Tatung University, Taipei 104, Taiwan
[3] Advanced Photon Source, Argonne National Laboratory, Argonne, IL 60439, USA
[4] Department of Engineering Science and System, National Tsing Hua University, Hsinchu 300, Taiwan
[5] Institute of Optoelectronic Sciences, National Taiwan Ocean University, Keelung 202, Taiwan
[6] National Synchrotron Radiation Research Center, Hsinchu 300, Taiwan
[7] X-ray Imaging Center, Pohang University of Science and Technology, Pohang 790-784, Korea
[8] Ecole Polytechnique Fédérale de Lausanne (EPFL), CH-1015 Lausanne, Switzerland

E-mail: giorgio.margaritondo@epfl.ch

Received 29 June 2008, in final form 21 July 2008
Published 8 August 2008
Online at stacks.iop.org/Nano/19/395302

Abstract
The fabrication of devices to focus hard x-rays is one of the most difficult—and important—challenges in nanotechnology. Here we show that Fresnel zone plates combining 30 nm external zones and a high aspect ratio finally bring hard x-ray microscopy beyond the 30 nm Rayleigh spatial resolution level and measurable spatial frequencies down to 20–23 nm feature size. After presenting the overall nanofabrication process and the characterization test results, we discuss the potential research impact of these resolution levels.

The nanofabrication of hard x-ray Fresnel zone plates (FZPs) is a very difficult task because of extreme and conflicting technical requirements [1–5]. Spatial resolution requires very thin outermost zones. However, high efficiency with weakly absorbed hard x-rays imposes a high aspect ratio. The reconciliation of such requirements is problematic: stable thin nanostructures with high aspect ratio are difficult to fabricate. As a result, progress was so far limited to soft x-rays [3] and the spatial resolution for hard x-rays remained above 40–50 nm [6, 7]. This is regrettable since it rules out many important applications in biomedical research, most notably subcellular structure studies in tissues.

We show here that by direct electron beam writing and a careful optimization of crucial processing parameters we obtained Au FZPs for >8 keV photon energy delivering a Rayleigh criterion spatial resolution of 29 nm in full-field imaging. Most important was the ad hoc adjustment of the duty cycle of the Au nanostructure to compensate for the line distortion induced by the resist development and electrodeposition. We cross-validated the spatial resolution with three different methods: the modulation transfer function (MTF) approach [8], power spectrum analysis (PSA) [9, 10] and practical microscopy tests coherently demonstrated the aforementioned resolution level.

Efficiency is another good characteristic of our FZPs: it exceeds 6% at 8 keV, substantially better than competing

[9] Author to whom any correspondence should be addressed.

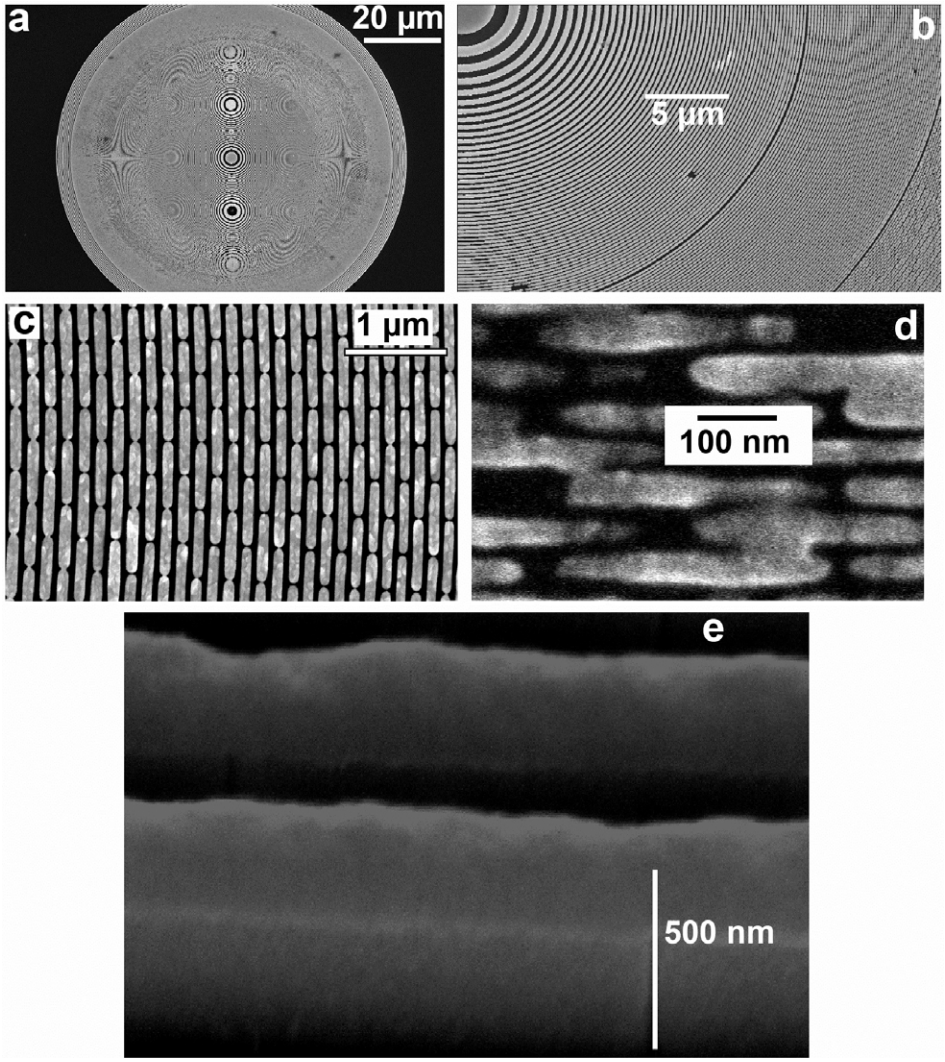

Figure 1. Scanning electron micrographs of an Au FZP with 30 nm outermost zone and >450 nm thickness. The regions and scale bar lengths were: (a) the complete zone plate, 20 μm; (b) the central zones, 5 μm; (c) the 40–50 nm zone width region, 1 μm; (d) the <30 nm zone width region, 100 nm; (e) a cross-sectional view, 500 nm.

devices with worse spatial resolution. Such an efficiency level is not far from the theoretical limit [11].

The structure of our FZPs consists of a gold pattern over a 1 μm thick silicon nitride membrane. The membrane was obtained with low pressure chemical vapor deposition (LPCVD) on a research-grade Si(100) wafer. The backside was etched by KOH to remove silicon until only the membrane was left. Then, we deposited a 5 nm Cr buffer layer and a 12 nm gold layer. Photoresist (polymethyl methacrylate, PMMA A6) was used to spin-coat the metal-covered membrane and then thermally cured at 170 °C for 15 min.

Electron beam writing (with an Elionix ELS-7000 system operating at 100 keV and 10 pA) followed, realizing a specially designed FZP pattern. This was based on a broken-line configuration [6] to avoid the collapse of the developed photoresists due to the high aspect ratio. As already mentioned, the pattern shape was empirically optimized by trial-and-error adjustments of the duty cycle, offsetting line distortion effects.

The e-beam dose was also empirically optimized, a difficult but critical step that cannot be automatically implemented. The photoresist pattern was developed with a 7:3 mixture of IPA (isopropanol) and water for 60 s to completely remove the e-beam exposed parts [6]. The final metal nanostructure was obtained by gold electrodeposition in the open trenches of the resist pattern. Details of the electrodeposition procedure—similar to an LECD (localized electrochemical deposition) approach—can be found in [6].

This procedure yielded the Au FZPs used in this study with the following key features of the gold nanostructures. The overall FZP pattern diameter was 82.6 μm, the width of the outermost zone was 30 nm and the metal nanostructure thickness was 450 nm. Therefore, the aspect ratio was $450/30 = 15$, producing the aforementioned efficiency level. Figure 1 shows scanning electron micrographs of a typical FZP fabricated with our method.

The FZP performances were characterized using a full-field transmission x-ray microscope (TXM) at beamline 32-ID of the Argonne Advanced Photon Source (APS) [5]. We used a rather large x-ray magnification 130× to minimize the effects

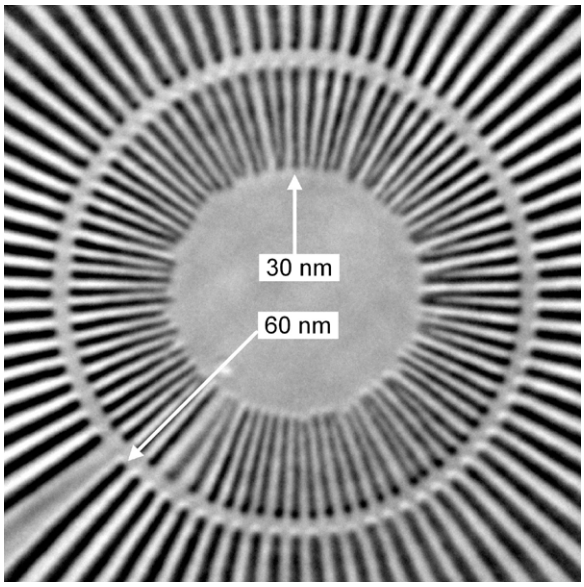

Figure 2. X-ray micrograph of a commercial Siemens resolution pattern obtained with our best hard x-ray FZP.

of the point spread function of the detector (CCD) system on the TXM spatial resolution. Indeed, the detector contribution to the TXM image resolution was <8 nm.

Figure 2 is a TXM image of a commercial Siemens start pattern consisting of 180 nm thick Au on a silicon nitride window. The narrowest lines in the center are 30 nm wide (i.e. with 60 nm period). Their tips are clearly visible, already suggesting a spatial resolution better than 30 nm.

More stringent tests of the <30 nm resolution were performed with a special test pattern fabricated at Academia Sinica, whose SEM image is shown in figure 3(a). The thinnest lines are <20 nm wide—and some of them can be distinguished in the x-ray image shown in figure 3(b). This again indicates a resolution level below 30 nm.

A first quantitative evaluation was performed by MTF analysis, measuring the intensity modulations in a number of line scans across objects with different widths. The intensity modulation is defined as $(I_H - I_L)/I_H$, where I_H is the intensity in regions between two Au lines and I_L is the intensity at the center of an Au line. The experimental uncertainty was estimated by sampling a large number of line scans for different parts of the test pattern. Figure 4 (round dots) shows the results: an MTF plot for the Academia Sinica pattern, where the intensity modulation was normalized to the absorption of 150 nm thick Au.

Based on the Rayleigh criterion, the spatial resolution is equal to the feature size (or to one-half of the line spacing period) for 26.5% intensity modulation. The result for the round-dot data in figure 4 is 29 nm. We performed the same MTF analysis for different resolution patterns: the Rayleigh resolution varied within 0.5 nm, always remaining below 30 nm. We also show for comparison in figure 4 (square dots) the MTF results for a zone plate with 45 nm outermost zone width and 900 nm thickness, obtaining a poorer Rayleigh resolution of 38 nm [5].

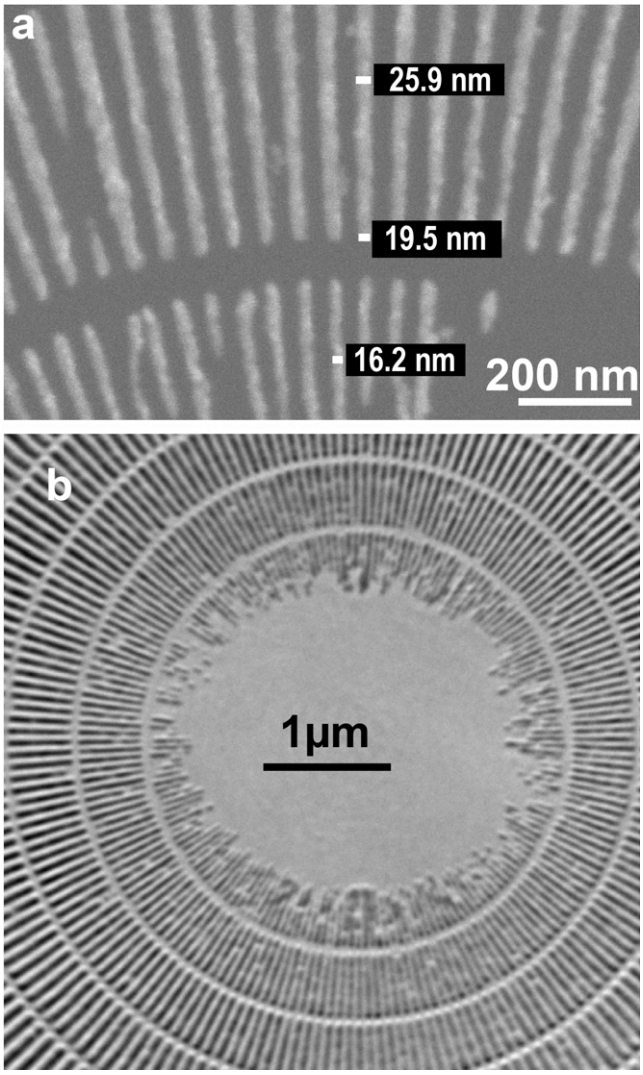

Figure 3. (a) SEM micrograph of a resolution pattern fabricated at Academia Sinica, showing the central area with the smallest lines of width <20 nm. (b) X-ray micrograph of the same pattern demonstrating the visibility of features smaller than 20 nm. Scale bar: 1 μm.

The MTF analysis is widely accepted and its interpretation is straightforward—but it requires extremely well-defined test patterns that are progressively difficult to fabricate as the spatial resolution improves. We thus decided to corroborate the MTF analysis results with PSA (see the detailed procedure in [9]). Specifically, we performed a two-dimensional Fourier transformation of the x-ray image of figure 3(b). Then, we integrated the two-dimensional power spectral intensity azimuthally (i.e. along the circle) at a fixed radial frequency.

Figure 5 shows the power spectrum for (A) the raw image of the object and (B) the background taken without the object. The power spectral intensity for the background monotonically decreases without fine structure as the frequency increases. In contrast, the power spectral intensity of the object exhibits strong features especially at low frequencies due to the different feature sizes. At high frequencies the object produces a monotonically decreasing intensity equivalent to that of the background.

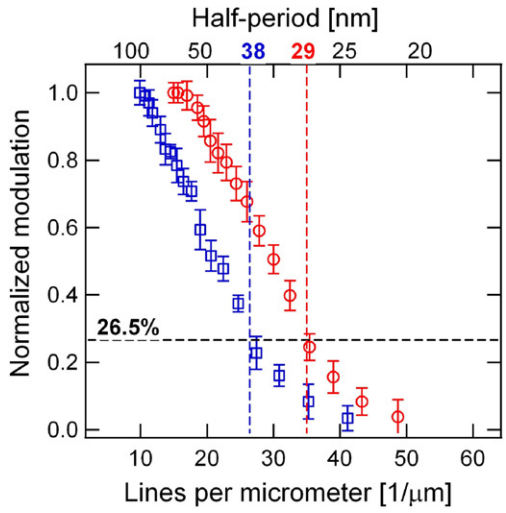

Figure 4. Measured modulation transfer function (MTF) used to evaluate the resolution level: plot (red open circles) of the measured intensity modulation as a function of the number of lines per unit length from images obtained using our best FZP (with 30 nm outermost zone width). The dashed line corresponds to the 26.5% modulation level, used for the evaluations based on the Rayleigh criterion. The interpolation of data points yields a resolution of 29 nm. For comparison, the same analysis gives a Rayleigh resolution of 38 nm for a different zone plate with 45 nm outermost zone width (blue squares).

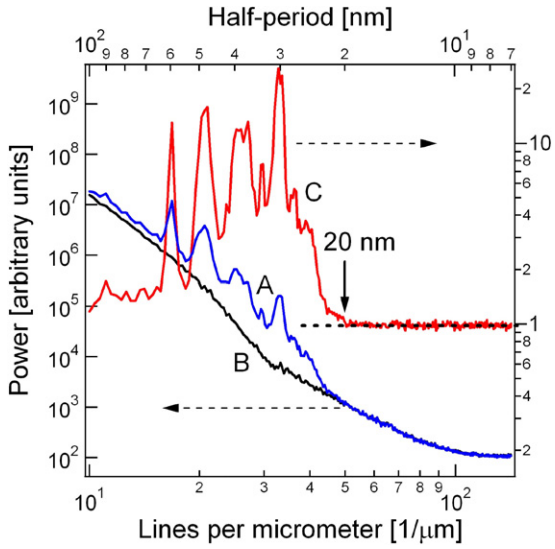

Figure 5. Power spectra obtained from (A) the raw image in figure 3 (blue) and (B) the background (black). The red curve (C) is the ratio of (A) over (B). The arrow indicates the onset of the power spectrum intensity above the background that corresponds to a minimum detectable feature size of 20 nm.

The differences between the two curves are emphasized by their ratio (plot (C)). At high frequency, the intensity is structureless, indicating that the image produces only noise. Below a threshold frequency corresponding to a half-period ≈20 nm, the curve reflects the object morphology. This demonstrates that the smallest object feature size with non-zero contrast is 20 nm. This is an important conclusion that is extremely difficult to reach using the MTF analysis.

We performed the PSA analysis for a number of samples also including biological specimens, consistently obtaining a cutoff feature size of 20–23 nm. This small variation is of course due to the specific morphology of each specimen with different spatial frequencies and noise levels.

In conclusion, both MTF and PSA independently demonstrated resolution levels <30 nm for our best FZPs—and specifically a Rayleigh resolution below 30 nm and measurable spatial frequencies down to a feature size of 20 nm.

What made possible this achievement? Certain factors were essential: among them, we already mentioned the two empirical optimization procedures for the e-beam dose and for the pattern duty cycle. In addition, we note the high (100 keV) electron energy for e-beam writing and the use of current pulses for Au electrochemical deposition.

The high electron energy enabled us to focus the electron beam down to a 5 nm diameter and reduce backscattering-related problems. As to pulsed electrodeposition, the optimized parameters for our best FZPs were a 0.2 s pulse width, a 40 s pulse distance, room temperature and a current density of 0.5 ASD (ampere per square decimeter). Pulsed electrodeposition was specifically better [6] than DC electrodeposition in filling the narrow trenches of the outermost FZP zones.

The optimized nanofabrication procedure enabled us to achieve the required FZP characteristics not only for resolution but also for efficiency. The resolution only depends on the outermost zone width whereas the efficiency depends on the metal structure thickness. For an Au FZP with 100 nm Au thickness, the efficiency would be only 0.1%; in contrast, at 8 keV photon energy the theoretical efficiency reaches ∼20% for a ∼500 nm thickness. The efficiency is important not only for time-resolved applications but also to reduce negative effects, for example, of vibrations and background inhomogeneities—a limited photon flux leads to long exposure times that worsen such effects. The thickness and the accuracy of the zone structures are also important when using high-order magnification [6].

The importance of finally reaching a <30 nm spatial resolution level in full-field hard x-ray microscopy needs not be emphasized. The potential impact touches many different areas: materials science, microelectronics, nanophotonics, the life sciences and other domains. Our demonstration that features <20 nm are easily visible opens the door, for example, to microradiology of subcellular details in thick tissue specimens, of deep DRAM features, of inside nanofeatures in fuel cells and of many other fundamental and/or technological objects.

Acknowledgments

This research was supported by the National Science and Technology for Nanoscience and Nanotechnology, the National Synchrotron Radiation Research Center (Taiwan), the Creative Research Initiatives (functional x-ray imaging) of MOST/KOSEF, the Fonds National Suisse pour la Recherche

Scientifique, the EPFL and the Lausanne Center for Biomedical Imaging (CIBM). The Core Facility for Nanoscience and Nanotechnology and Biomedical NanoImaging at Academia Sinica is acknowledged for the use of the equipment. Use of the Advanced Photon Source is supported by the US Department of Energy, Office of Sciences, Office of Basic Energy Sciences, under contract no. DE-AC02-06CH11357. The authors thank Dr Stefan Vogt for useful discussions.

References

[1] Yun W, Lai B, Krasnoperova A, Di Fabrizio E, Cai Z, Cerrina F, Chen Z, Gentili M and Gluskin E 1999 *Rev. Sci. Instrum.* **70** 3537

[2] Attwood D 1999 *Soft X-Rays and Extreme Ultraviolet Radiation: Principles and Applications* (Cambridge: Cambridge University Press) p 337

[3] Lo T N *et al* 2007 *J. Phys. D: Appl. Phys.* **40** 3172

[4] Chao W, Harteneck B D, Liddle J A, Anderson E H and Attwood D T 2005 *Nature* **435** 1210

[5] Chen Y T *et al* 2008 *J. Synchrotron Radiat.* **15** 170

[6] Yin G C, Song Y F, Tang M T, Chen F R, Liang K S, Duewer F W, Feser M, Yun W and Shieh H P D 2006 *Appl. Phys. Lett.* **89** 221122

[7] Chu Y S *et al* 2008 *Appl. Phys. Lett.* **92** 103119

[8] Chao W, Anderson E, Denbeaux G P, Harteneck B, Liddle J A, Olynick D L, Pearson A L, Salmassi F, Song C Y and Attwood D T 2003 *Opt. Lett.* **28** 2019

[9] Vogt S, Schneider G, Steuernagel A, Lucchesi J, Schulze E, Rudolph D and Schmahl G 2000 *J. Struct. Biol.* **132** 123

[10] Neeff T, Dutra L V, Santos J R D, Freitas C C and Araujo L S 2005 *J. Remote Sensing* **26** 13

[11] Michette A G, Buckley C J and Pfauntsch S J 1997 *Opt. Commun.* **141** 118